SANDIA REPORT

SAND2004-1485
Unlimited Release
Printed May 2004

Using a Dynamic Point-Source Percolation Model to Simulate Bubble Growth

D. Zeigler, J. Zimmerman, D. Cowgill

Prepared by
Sandia National Laboratories
Albuquerque, New Mexico 87185 and Livermore, California 94550

Sandia is a multiprogram laboratory operated by Sandia Corporation,
a Lockheed Martin Company, for the United States Department of Energy's
National Nuclear Security Administration under Contract DE-AC04-94AL85000.

Issued by Sandia National Laboratories, operated for the United States Department of Energy by Sandia Corporation.

Available to DOE and DOE contractors from
U.S. Department of Energy
Office of Scientific and Technical Information
P.O. Box 62
Oak Ridge, TN 37831

Telephone: (865)576-8401
Facsimile: (865)576-5728
E-Mail: reports@adonis.osti.gov
Online ordering: http://www.osti.gov/bridge

Available to the public from
U.S. Department of Commerce
National Technical Information Service
5285 Port Royal Rd
Springfield, VA 22161

Telephone: (800)553-6847
Facsimile: (703)605-6900
E-Mail: orders@ntis.fedworld.gov
Online order: http://www.ntis.gov/help/ordermethods.asp?loc=7-4-0#online

SAND2004-1485
Unlimited Release
Printed May 2004

Using a Dynamic Point-Source Percolation Model to Simulate Bubble Growth

David A. Zeigler
Jonathan A. Zimmerman
Science-Based Materials Modeling Department

Donald F. Cowgill
Engineered Materials Department

Sandia National Laboratories
P.O. Box 969
Livermore, CA 94551

Abstract

Accurate modeling of nucleation, growth and clustering of helium bubbles within metal tritide alloys is of high scientific and technological importance. Of interest is the ability to predict both the distribution of these bubbles and the manner in which these bubbles interact at a critical concentration of helium-to-metal atoms to produce an accelerated release of helium gas. One technique that has been used in the past to model these materials, and again revisited in this research, is percolation theory. Previous efforts have used classical percolation theory to qualitatively and quantitatively model the behavior of interstitial helium atoms in a metal tritide lattice; however, higher fidelity models are needed to predict the distribution of helium bubbles and include features that capture the underlying physical mechanisms present in these materials.

In this work, we enhance classical percolation theory by developing the dynamic point-source percolation model. This model alters the traditionally binary character of site occupation probabilities by enabling them to vary depending on proximity to existing occupied sites, *i.e.* nucleated bubbles. This revised model produces characteristics for one and two dimensional systems that are extremely comparable with measurements from three dimensional physical samples. Future directions for continued development of the dynamic model are also outlined.

Keywords: percolation theory; helium; bubbles; nucleation; growth; accelerated release.

This page intentionally left blank.

Contents

List of Figures

This page intentionally left blank.

1 Acronyms and Symbols

D	fractal dimension
DPSP	dynamic point-source percolation
E	Euclidean dimension of a lattice
FCC	face centered cubic
He	helium
HK	Hoshen-Kopelman
$M(L)$	number of sites belonging to the largest cluster on a LxL sublattice
M	metal
MC	Monte Carlo
MD	molecular dynamics
NMR	nuclear magnetic resonance
NZ	Newman-Ziff
$P(p)$	percolation probability, the probability that an occupied site is part of an infinite cluster
$P_\infty(p)$	same meaning as $P(p)$
$P_N(p)$	probability that an occupied site is part of a cluster of N sites
p	site occupation probability
p_c	critical site occupation probability, percolation threshold
q	site availability, equal to the value of $1 - p$
R_g	radius of gyration of a cluster
s	number of sites in a cluster
$S(p)$	mean cluster size for occupation probability p
S	size of the sphere of influence
SOI	sphere of influence
TEM	transmission electron microscopy

This page intentionally left blank.

2 Introduction

The nucleation, growth and interaction of helium (He) bubbles in metal hydride materials is of high scientific and technological importance. Helium is present in these systems due to the use and decay of tritium. Since He is insoluble in metals, the He atoms accumulate in the material and cluster, leading to the formation of nano-scale bubbles that grow as the concentration of He within the metal increases. Such bubbles have been observed experimentally within palladium [1, 2] and vanadium [3] tritide alloys. A key phenomenon intricately tied to the presence of these bubbles is the observation of helium gas released from the alloy at an accelerated rate once a critical concentration of helium-to-metal atoms (He/M) is reached. For example, examination of aged palladium tritide samples has revealed that when the ratio He/M reaches values between 0.5 to 0.55 [4, 5], a large amount of ^{3}He is released. This critical ratio depends upon a number of factors, including microstructure, system temperature, and whether or not tritium replenishment occurs.

Engineering needs require the development of numerical models capable of predicting the characteristics of metal hydride systems when accelerated release of He gas begins. This sudden release of the He through the material is a trait of percolation models. Percolation theory was originally developed to describe how small branching molecules form larger and larger macromolecules if more and more chemical bonds are formed between the original molecules [6]. The first formal study of percolation theory was conducted by Broadbent and Hammersley [7] who introduced lattice models for the flow of a fluid through a static random medium. Furthermore, they showed rigorously that no fluid will flow if the concentration of active medium is smaller than some nonzero threshold value [8]. Another feature introduced was the notion of a percolation probability, the likelihood that any given region of the medium is sufficiently well connected to the rest to be available for conductance.

Percolation models have been formulated and used to provide understanding of the interaction of the helium within metal hydride lattices. Weaver and Camp [9] used percolation theory along with observations made with NMR, nuclear magnetic resonance, to hypothesize on mechanisms leading to detrapping of interstitial He within titanium tritides. Camp later extended this work [10] to show that the critical concentration for accelerated release of He for a host of CaF_2-structure ditritrides is independent of metal atom species. Spulak eventually used these early efforts to provide quantitative predictions of the critical release concentration, and compared these estimates with data gathered from observation of metal tritide thin films [11]. Ronchi [12] applied a bond percolation model to study the interlinking of bubble clusters. Massih [13] utilized a Monte Carlo simulation to obtain the fraction of interlinked bubbles as a function of the bubble concentration in the material. Although these efforts have been crucial in modeling the onset of accelerated release of He gas, more detailed numerical models are needed to predict the distribution and interaction of He bubbles at accelerated release, and characteristics related to the underlying physical processes

active when bubble linkage occurs (assuming that such a linkage is a precursor to accelerated release). In addition, recent advances in computer technology allow for percolation models to be used in a more powerful manner than in past efforts.

The goal of this work is to understand and model the evolution of the spacing distribution between He bubbles. This is accomplished by constructing a model based on percolation theory that possesses enhancements to closely simulate the nucleation, growth and clustering behavior of He bubbles. Section 2 provides a brief description of the classical percolation theory. Section 3 details the construction of the dynamic point-source percolation model specifically constructed to provide a model for bubble nucleation and growth within the classical percolation theory framework. The section closes with the application of the dynamic model to a one-dimensional and two-dimensional medium and the comparison with experimental data. Section 4 describes a modern treatment of percolation methods based on the use of fractals. Finally, section 5 provides a summary of the research presented in this report, and outlines future possibilities for continued development of the dynamic point-source percolation model.

3 Classical Percolation Theory

Percolation theory describes the behavior and properties of particles spreading through and interacting with a random medium. To clarify the terminology used for percolation theory, we define a *medium* as an infinite set of *sites* and the diffusing particles are the *fluid*. The fluid travels through the medium along paths or *bonds* connecting the sites. If a site is occupied by a fluid particle, then the site is said to be *wet*. The random process of fluid particles traversing the medium to occupy sites can be approached either as a "classical" diffusion problem or a percolation problem. In the diffusion problem, it is assumed that the fluid elements exhibit random motion in a constraint-free medium. As such, a diffusing particle may reach any position in the medium. Percolation problems are distinguished from diffusion problems by two crucial properties:

- the stochastic behavior is determined by the medium. Unlike the diffusion problem where the stochastic behavior is associated with the fluid particle, the medium dictates which pathways are available to the particles. This condition implies a topography to the medium. In essence, by restricting the flow of individual particles, flow channels and wells are created.

- the presence of a *percolation threshold*. By the property of the medium provided above, the possibility exists that the motion of every particle is constrained to a region of size smaller than the entire domain. That is, the fluid is not allowed to flow through the medium in an unconstrained fashion. Associated with each configuration is a scalar value called the percolation threshold, or *critical probability* as it is often referred to, which determines if the fluid is restricted to a finite region. The value of the percolation threshold represents the fractional number of sites that must be occupied in order for the fluid to wet sites over the entire span of the medium. Below this value, only finite regions of occupied sites exist and fluid cannot flow through the whole medium.

Percolation processes are similar to the diffusion process but represent fundamentally different physical mechanisms. A typical situation in which the diffusion process is valid is the motion of one molecule in a gas as it is scattered by other molecules. When the gas is sufficiently dilute, the 'memory' of previous collisions can be neglected in treating each scattering event as a random process, with a fixed distribution of results. When the scattering medium exhibits no memory, it is possible to think of the random scattering as a property of the one molecule studied. However, in the percolation process there is a distinction between the fluid and the medium. While the medium may vary in a random way spatially, it's randomness does not vary in time. Thus, memory effects cannot be neglected and the randomness is considered a property of the medium.

A simple example of the differences between percolation and diffusion theory is the Polya walk in one dimension [14]. Assume a medium which can be described by a set of points placed at unit intervals along a straight line. The particles of the fluid move in steps of unit length in either direction with equal probability. The process is diffusive when the direction of the step is chosen at random, with the medium playing a completely passive role (the left image in figure 1.) In the corresponding percolation process the fluid is the same as before, but this time the points defining the medium are labeled with arrows pointing either to the left or to the right with equal probability and a particle is required to move from a given point only in the direction of the arrow at that point (the right image in figure 1.) The motion of the particle is thus governed by the medium. In this percolation process a particle can get trapped and be forced to oscillate between two points whose arrows point towards each other, while the possibility of trapping does not exist in the diffusion picture. This

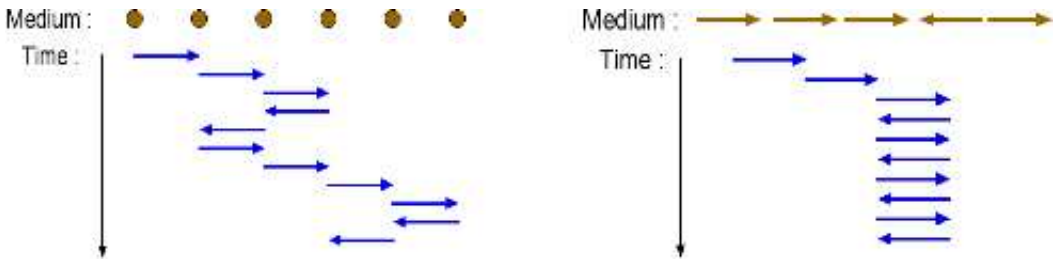

Figure 1: One-dimensional Polya walk. The left figure corresponds to a diffusive model where the medium is neutral and the particle has equal probability of moving left or right. The right figure is the percolation model. The medium dictates the particle displacement with equal probability of motion to the left or right. Notice that this configuration forms a well which traps the particle.

possibility of trapping, as well as the notion of blocking, defined as the inability for a fluid particle to move in the direction of particular sites, is what distinguishes percolation from diffusion.

Two distinct philosophies exist regarding how a percolation problem is conceived. These are the bond percolation model and site percolation model. These models are differentiated by associating the medium's properties with either the bonds or the sites, respectively. For example, consider the blocking of fluid particle motion through the medium. The bond percolation model would consider the bonds, the paths between sites, to be blocked. In contrast, the site percolation model considers the sites themselves to be blocked but the paths between sites to be unblocked. In this work, we use a site percolation model.

Each site has a probability p of being occupied. It is assumed that fluid is allowed to flow freely between any two adjacent wet (occupied) sites. The expression $P_N(p)$ is defined as the probability that a single arbitrary site is not only occupied, but is part of a cluster of

N sites that are connected and also occupied. The term "connected" here means that all the sites belonging to such a cluster are nearest neighbors with at least one other site also belonging to that same cluster. The probability of a site belonging to an infinite cluster is $P(p) = \lim_{N\to\infty} P_N(p)$. Theoretically, for a lattice of infinite extent an infinite cluster spans the entire lattice. This does not imply that all sites are occupied, but rather at least one pathway exists between occupied sites that extends to anywhere within the lattice. For a finite system with boundaries, the infinite cluster refers to a pathway that connects multiple boundaries of the system, e.g. top and bottom or left and right. $P(p)$ is called the *percolation probability*, but is also known as the gel fraction when dealing with liquid/solid problems. The critical probability for the lattice is defined as $p_c = \sup\{p|P(p) = 0\}$. That is, p_c is the least upper bound on the set of all p such that $P(p) = 0$. When $p < p_c$, all clusters are of finite size. Hence, no infinite cluster exists and $P(p) = 0$. When $p > p_c$, a cluster of infinite size is formed and a percolation channel exists, i.e. $P(p) \neq 0$. This corresponds to a change of state for the medium. Figure 2 shows the change from a medium which has finite clusters of fluid, thus creating a barrier for the fluid, to one that allows the fluid to pass through.

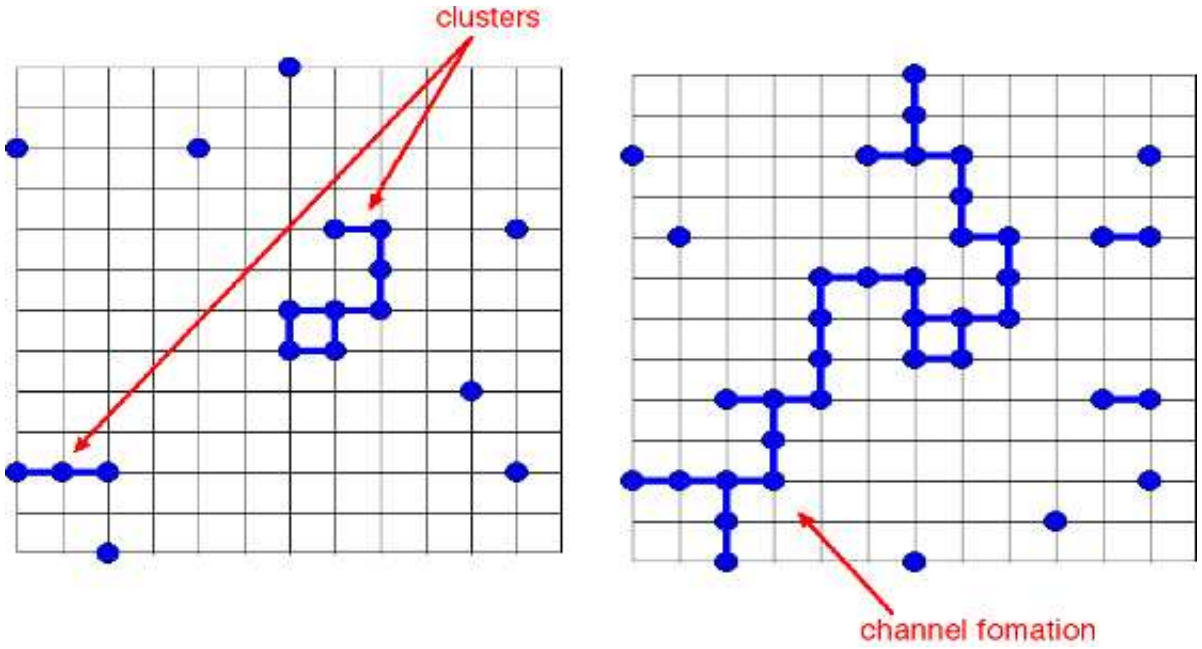

Figure 2: The left image shows a lattice with an occupation probability of ∼0.1259. Notice that fluid does not flow through the medium as all clusters are of finite size. The right image is an identical lattice with occupation probability of ∼0.2727. A cluster has formed which links the top and bottom borders indicating that fluid percolates through the medium.

The value of the critical probability, p_c, is dependent upon the geometry and the dimension of the lattice. It can be determined analytically, approximated by series expansion, or

calculated using a Monte Carlo simulation. Analytic techniques have been utilized primarily in two dimensional lattices. In fact, the critical probability values are known for triangular, square [15], honeycomb and Kagome [16] lattices. For generalized lattices, Sykes and Essam [17] employed a geometric argument to construct complementary lattice pairs, L and L^c. Denoting p_c and p_c^c as the critical probabilities of L and L^c, respectively, the matching property dictates that $p_c + p_c^c = 1$. D'Iribarne et. al. [18] utilized graph theory, through the minimal spanning tree, to determine site percolation thresholds for regular 2D lattices. Recently, an approach using preferred directions has been conjectured by Rosowsky [19]. This method begins with the existence of a fixed, "pivotal" site for which a change in status of the site from occupied to unoccupied would separate an infinite cluster into two finite and disconnected clusters. A set is constructed of all possible configurations of the infinite cluster. Then, a probability function $R(p)$ is computed to characterize this set. The approximate value of p_c corresponds to the maximum of $R(p)$ for the interval $]0, 1[$.

Determining p_c by series expansion relies upon estimating the mean cluster size, $S(p)$. At $p = p_c$, there is a finite probability for an infinite cluster to be formed. Therefore, as p approaches p_c from values less than p_c, $S(p)$ must become infinite. Assuming that $S(p)$ can be expressed as the series summation $S(p) = \sum_n a_n p^n$, the series diverges as $p \to p_c$. The radius of convergence for the power series gives a lower bound for p_c. Because of the complexity of these series, numerical evaluation is often used.

The Monte Carlo approach is based upon the method of the same name used to simulate thermal systems [20], although it is much simpler due to the random nature of the percolating medium. For a particular lattice and set occupation probability, p, a lattice profile is constructed by evaluating the occupied status at each site. This is accomplished by selecting a random value, r, over the unit interval, $[0, 1]$ at each site. If $r \geq p$ then the site is occupied; otherwise the site remains empty. Note that this dictates that the maximum occupation density of the lattice will be p. Once each site has been evaluated, one may analyze the lattice to check whether a channel is formed. Repeating this several times provides an estimate for $P(p)$ to be the ratio of the number of configurations which yielded channel formation over the total number of evaluated configurations. By definition, p_c is the largest value of p such that $P(p)$ is zero. The most computationally intensive portion of this method is the determination of channel formation, and special algorithms must be used to perform this task. Several algorithms [21, 22] have been developed to efficiently count the clusters and determine the percolation status. The Hoshen-Kopelman (HK) algorithm [23] is a simple algorithm that utilizes labeling clusters. Unfortunately, the HK algorithm examines lattice sites with regard to channel formation in a preferred direction and only evaluates the lattice for a static value of p. Moreover, for large lattices, the memory required to analyze the lattice could exceed that available by the computer.

A more efficient algorithm which does not have the limitations of the HK algorithm is the Newman-Ziff (NZ) algorithm [24, 25]. The NZ model is more versatile than previous models

in that it allows one to change p on the fly and utilizes a "union-find" algorithm (also known as the "weighted union-find with path compression" [26]) to generate cluster trees that decreases the memory requirements of the simulation. Each cluster is represented as a tree with a pointer to a root site. When an occupied site is encountered, the clusters to which the site belongs are identified by traversing the respective trees until the root sites are found and then, if necessary, amalgamating the trees. This amalgamation takes place by making the smaller tree a subtree of the larger, called "weighting", and by changing the pointers of all sites along the tree path traversed to reach the root site to point directly to the root, called "path compression". The Newman-Ziff model boasts the powerful advantage of being an $\mathcal{O}(N)$ algorithm, meaning that calculation time for determining system property values for the entire range of occupation probabilities, $0 \leq p \leq 1$, is proportional to N, the number of lattice sites that comprise the system.

This page intentionally left blank.

4 Dynamic Point-Source Percolation Theory

While classical percolation theory has enjoyed much success, it possesses many characteristics that make it inadequate to accurately model He bubble growth. For example, the classical model assumes that the system is in a static state of equilibrium. Also, the occupation probability, p, is assumed to be constant and uniform over the entire lattice. Moreover, the percolation mechanism is purely stochastic and does not capture the underlying physics of the system. This random approach restricts the manner in which occupied sites are selected to a single methodology.

To address these issues, a new approach to the percolation model must be considered. The main focus of any alterations to the classical theory is to gain the ability to reproduce observed physical behavior in simulated systems. The growth pattern of the He clusters to form channels using bubble growth is substantially different than a collection of random sites. The bubble growth mechanism may lead to lower critical probability values than those determined using classical theory. Another issue is the placement of the occupied sites. As bubbles form in the medium they are more likely to nucleate with maximal spacing from other occupied sites. Thus, the random process of determining occupation sites is weighted towards vacant sites. To surmount these issues, the dynamic point-source percolation model (DPSP) is introduced as a new approach to percolation theory that features a dynamically changing occupation probability field associated with the lattice and a two-step percolation mechanism reflecting distinct cluster behavior.

4.1 Methodology

Suppose that the medium can be described using a lattice, $L = \{l_{ijk} | i \in I, j \in J, k \in K\}$, embedded in $\mathbb{R}^3$ where I, J and K are finite subsets of $\mathbb{Z}$, the set of all integers. Thus, each site in the medium is associated with a lattice point, l_{ijk} and vice-versa. Since $L \subset \mathbb{R}$, l_{ijk} can be expressed using the ordered triple (x_i, y_j, z_k) for every i, j, k. Let us denote M to be the smallest convex subset of $\mathbb{R}^3$ containing L and define the piecewise analytic function, $p : M \to [0, 1]$. $p(l_{ijk})$ represents an occupation probability associated with site l_{ijk}. At the start of the percolation process, all sites are available to become occupied; hence, $p = 0$ for all sites. If site l_{ijk} becomes occupied, then $p(l_{ijk}) = 1$ and it is assumed a bubble has nucleated at that site. Once a site is occupied, the occupation probability of all neighboring sites within a specified distance, referred to as the site's sphere of influence (SOI), are modified by a potential function. This function alters the value of p for all neighboring sites to lie within the interior of the interval $]0, 1[$. The dependency of p as a function of distance from a fully occupied site is determined by the process being modeled. Either way, for a pair of sites separated by a large distance, the action of one lattice point being occupied will

have little influence on the occupation probability of the other, a characteristic consistent with physical behavior. The value for p is dynamic in that as a site becomes occupied, the occupation probability field reflects the change. Figure 3 depicts the 3-dimensional surface and 2-dimensional contour plots of the occupation probability over a two dimensional lattice with 3 occupied sites. In a sense, the variable p has now taken on a special meaning. Not

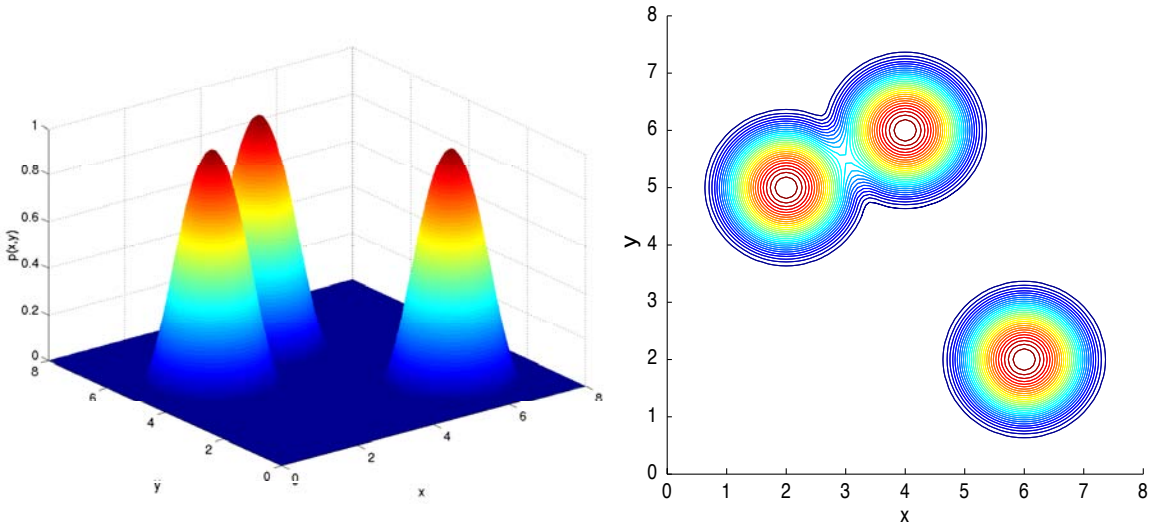

Figure 3: 3-dimensional surface (left) and 2-dimensional contour (right) plots of the occupation probability, p, over a two dimensional lattice of 8 square units with three randomly selected nucleation sites. The occupied sites are located at (2,5), (4,6) and (6,2). Each site has a SOI value of 1.5.

only does it represent the probability that a site is occupied, but its inverse $q \equiv 1 - p$ can be considered the probability associated with the possibility of future occupation. Hence, once a site is filled, $p = 1$ and $q = 0$, not only can it not be filled again, but neighboring sites have a low probability of becoming occupied.

As mentioned above, cluster growth is modeled using a two-step process. The first step, nucleation, uses the occupation probability field to select nucleation sites for the He bubbles in the medium. As nucleation sites are chosen (site occupation), the occupation probability field changes dynamically, affecting subsequent nucleation. This stage concludes when a prescribed occupation density is attained ($\sim$10 ppm.) Upon the conclusion of the nucleation stage, the growth stage begins which is characterized by the growth of each nucleated site. The simulation concludes when a channel of connected bubbles is formed through the lattice.

4.1.1 Nucleation

The nucleation stage is characterized by the clustering of He within the metal lattice, leading to the formulation of nano-scale bubbles. This clustering is caused by the mechanism of self-trapping of He atoms [27]. At moderate concentrations of He, on the order of 1 ppm or greater, mobile He atoms encounter one another with enough regularity that they form small clusters of 2 to 5 atoms that are energetically favorable to remaining separated. At this point, self-interstitial defects of the metal form and remain in close proximity to, but non-uniformly distributed around, the He cluster. As some or all of the He atoms "fall into" the conjugate vacancies created by the metallic self-interstitial, their mobility is decreased and it can be considered that a bubble has formed. The strain field produced by the combination of the existing He cluster and the metallic self-interstitial defects, along with binding energetics of the trapped He, promote further trapping of He atoms to the bubble. This mechanism of self-trapping provides the physical reasoning for use of the SOI; a lowering of the mobile or diffusing He concentration occurs in the vicinity of existing He bubbles, and the probability for the nucleation of a new bubble (q) is proportional to the square of this decreased concentration.

As the distribution of locations where this self-trapping and subsequent bubble nucleation occurs is initially random, the fundamental mechanism in the numerical simulation is largely stochastic but favors regions of the lattice that possess a lower density of occupied sites. The first step in the process is to randomly select a potential nucleation site from the candidate list of unoccupied sites. Influencing the choice of candidate sites is the occupation probability field, p. At the inception of the nucleation stage, the lattice is empty in that none of the sites are occupied. This corresponds to a uniform occupation value of zero, $p(l_{ijk}) = 0 \ \ \forall \, l_{ijk} \in L$. That is, each site of the lattice is equally likely to be settled by an individual He atom. Once a random site is filled in, the magnitude of p rises to 1 at the site. Lattice points within the occupied site's SOI are also modified by a prescribed potential function.

Because of the presence of a filled site, the selection of subsequent candidate sites is not as simple as randomly selecting a lattice point. Once a candidate site is chosen, there is a chance that the lattice point is an undesirable location for nucleation. For example, a candidate site near an already occupied site is less likely to be a nucleation site than one remotely located from filled lattice points. The value for p determines whether a candidate site is "accepted" as a nucleation site. Once a candidate site is found, a randomly selected value, referred to as the acceptance probability, is compared against p. The site is then a nucleation site if the acceptance probability is greater than p at that site. Hence, for the initial step where the lattice is empty, since $p = 0$ then any candidate site is automatically a nucleation site. As the simulation progresses, it becomes more difficult to form nucleation sites due to the saturation of occupied sites in the medium. In fact, the nucleation stage concludes once a prescribed density of nucleation sites is attained, approximately 10 ppm. This value is determined by matching the bubble density of the simulated system to physical

measurements of bubble densities made with transmission electron microscopy (TEM).

4.1.2 Growth

Once the nucleated He bubbles have settled in the metal, as the concentration of He increases the He bubbles grow. This continues until a critical concentration of He-to-metal atoms is reached and gas is released from the material at an accelerated rate. The growth stage is marked by a distinct change in the methodology with which sites are occupied. Each nucleation site is a He bubble and additional He will act to enlarge the bubble rather than form new nucleation sites. Hence, each nucleation site can be considered as a root element of a cluster containing at least one element. To simulate bubble growth, at each time step, each cluster is allowed to absorb neighboring unoccupied sites in a distinct growth pattern. As distinct bubbles (clusters) merge, they form larger clusters which eventually grow to form a channel.

For example, assume every nucleation site has a growth pattern described by unit rate spherical growth. That is, for time step t, the elements of each cluster are the lattice sites located within t units of the root site. At each nucleation site, after the first time step the cluster will contain all sites within a distance of 1 unit from the root element; after the second step the cluster will then contain all sites within a distance of 2 units from the root element; etc. Eventually, this process will continue until the bubbles grow together to form a channel. In the simulation, we would also want to scale the growth rate of each root site according to the lattice source volume it encompasses, with larger spacings between root sites leading to more rapid growth.

4.2 Numerical Code

At the time of this writing, our numerical code has only been developed sufficiently to simulate the nucleation stage for lattices with a regular rectangular geometry. Note that by taking a sufficiently small nodal spacing, generalized lattice geometries can be approximated by embedding them into a regular lattice.

4.2.1 One-dimensional Model

The one dimensional model was first studied by Cowgill [28]. Assume a line with lattice points separated by a unit distance. An initial distribution of bubble spacing is specified by a function $f(x)$ where the random variable, x, represents the bubble spacing, i.e. the SOI is

$x/2$ units. The SOI is consistently maintained to be half the distance between occupied sites. For each bubble, the occupation probability within the SOI is determined by the ratio of available nucleation sites with total nucleation sites. Since this is a one dimensional model, for spacing x the nucleation probability within the SOI is $p = [(x-1)/x]^2$. Suppose that a new bubble nucleates y units from a bubble with SOI x. Then a new bubble forms of SOI $y_1 = y/2$ units while the SOI of the adjacent bubbles shrink to $y_2 = (x+y)/2$ and $y_3 = x - y/2$. The bubble spacing distribution is then adjusted by adding the probability of the spacing values, y_i, $i = 1, 2, 3$, created from the original spacing x by the formulation,

$$\begin{aligned} f(y_1) &= f(y_1) + pf(x) \\ f(y_2) &= f(y_2) + pf(x) \\ f(y_3) &= f(y_3) + pf(x) \\ f(x) &= f(x)(1-2p). \end{aligned}$$

A schematic of this process is shown in figure 4. In effect, this algorithm takes bubbles of

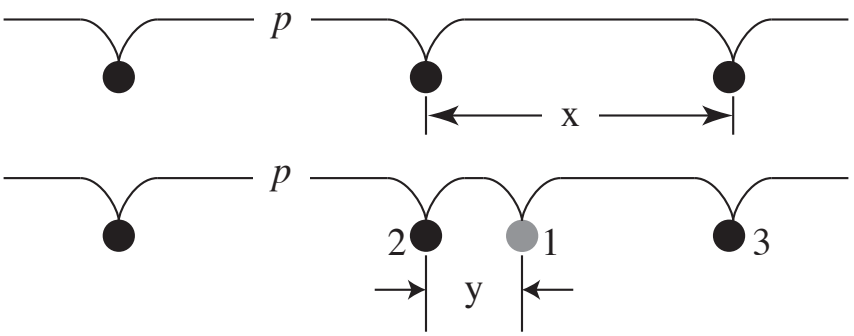

Figure 4: The one dimensional bubble nucleation model. (Top) Initially, bubbles are uniformly spaced at a separation distance, x, and have an associated nucleation probability field, p. (Bottom) When a new bubble is nucleated at a distance y from an existing bubble, the probability field changes accordingly and the spacing distribution function is recalculated.

larger radii and replaces them with multiple bubbles of smaller size. It is assumed that if bubbles are sufficiently close together they would merge to form a larger bubble. Hence, a minimal bubble spacing distance is enforced. This one dimensional model is slightly different from the theory described in the previous section in that the occupation probability field p associated with each occupied site is changed through modification of the dimension of the SOI when a new bubble is nucleated. This is somewhat different from superposing the occupation probability fields of many bubbles in close proximity to one another, the conceptual model to be used in multiple dimensions and to be discussed in the next section, but has a similar end result.

This model was applied to a 100 unit length lattice. It was assumed that the lattice was

initially empty, represented by setting f to be unity at 100 and 0 elsewhere. The appearance of the spacing distribution is shown in figure 5 after nucleating 500 bubbles.

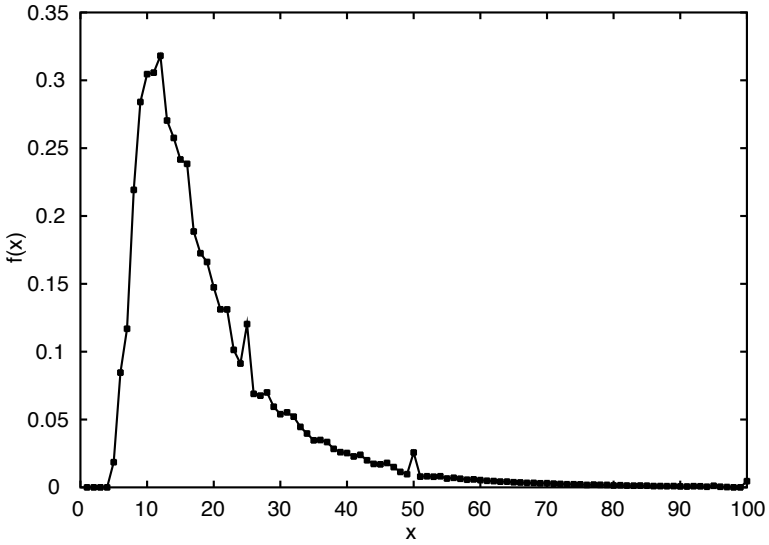

Figure 5: Bubble spacing distribution after nucleating 500 bubbles in a 1D lattice of 100 unit length. The minimal bubble spacing is approximately 5 units

4.2.2 Two-dimensional Model

It is the goal of this study to be able to study percolation via bubble growth using generalized lattice geometries. Early attempts at creating the simulation for generalized geometry were faced with slow performance due to substantial I/O calls to the hard drive to store and recall lattice geometry information during runtime. While smaller lattices ($\leq$2000 sites) performed adequately by storing all geometry information in dynamic arrays, these were too small to be informative. Regardless of lattice size, dynamically updating all nodal data once a bubble had nucleated slowed performance time. Consequently, it was decided that a regular lattice with unit spacing would provide a solid foundation since all geometry information is known by analytic argument, thereby requiring minimal memory during the execution of the simulation. Storing occupied sites requires only recording the index associated with each site and the Euclidean coordinates can be explicitly determined. Furthermore, the lattice size is only restricted by the range of integer values allowed by the processor.

The sites of the lattice are labeled by a sequential subset of the natural numbers, $\mathcal{N} \subset \mathbb{N}$. Starting in the lower left corner of the lattice, label the first site "1", the site adjacent to the right as "2", etc. until the end of the row is reached. Indexing is resumed at the left-most

site of the row immediately above. All geometric data is known for each site simply by the index value. Furthermore, since the size of the lattice is already known, explicit information concerning individual site locations in 2-space and neighbors is not needed. Subsets of the lattice are also indexed by $\mathcal{N}$. For example the collection of occupied sites is a dynamically allocated array of indices which resides in memory. The occupation probability function, p, can then be generated on the fly using the indices of nucleated bubbles. After each nucleation step, the array of nucleated sites can be recorded to the hard drive. By assuming the SOI radius is uniform throughout the lattice, each file generated only needs to store the list of indices corresponding to nucleated sites. For a lattice of, say, 10^9 lattice points, at the conclusion of nucleation when the density is approximately 10 ppm, all that is required is to store an array of 10^4 integer values. It should also be noted that this approach can be easily adapted to accommodate lattices in higher order spaces.

Suppose that the medium can be described using a regular rectangular lattice of M rows and N columns. Each site is represented as (i, j) where $i = 1, \ldots, M$ and $j = 1, \ldots, N$. Consider the case where $M = N = 10,000$. For a final occupation density of 10 ppm the profile at the conclusion of the nucleation stage is seen in figure 6. For this simulation, the

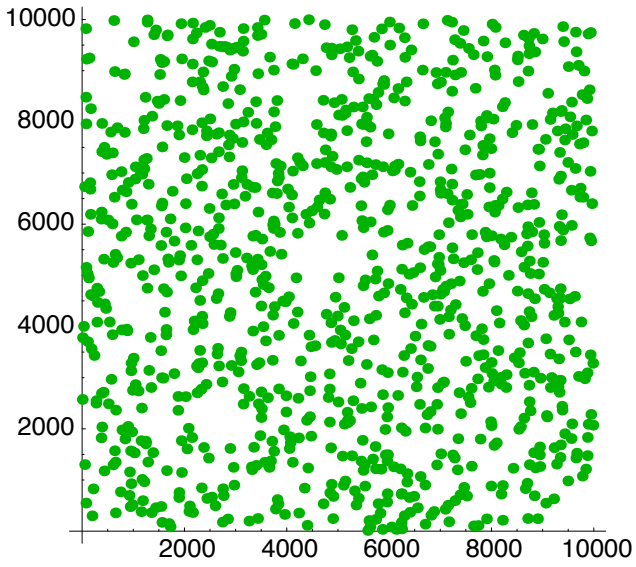

Figure 6: The profile for a 10,000 x 10,000 site lattice with a final occupation density of 10 ppm at the conclusion of the nucleation stage. Using serial code on a single processor this calculation required ∼480 seconds.

probability function used was

$$p = 1 - \prod_{i=1}^{n} \hat{q}\,(r_i), \tag{1}$$

where

$$\hat{q}\left(r_i\right) \equiv \begin{cases} 0 & \text{if } r_i < 1, \\ (1 - \frac{1}{r_i^3})^2 & \text{if } 1 \leq r_i \leq S, \\ 1 & \text{if } r_i > S. \end{cases} \tag{2}$$

and r_i represents the distance between the chosen site being evaluated and one of the remaining neighbor sites, $i = 1, 2, \ldots, n$, within the chosen site's SOI that are occupied. In the expression for $\hat{q}\left(r_i\right)$, S is the size of the SOI. The function given in equations (1) and (2) has the property that for a given site, if one or more nearest neighboring sites are already occupied, it will possess a very high occupational probability and is unlikely to be filled in the future. For example, if the site is a nearest neighbor to a single occupied site, it's value for p equals 0.9999. If the site is second nearest neighbors to the occupied site, with a distance r_i equal to $\sqrt{2}$, the value of p is approximately 0.5775. The value chosen for S was 5, effectively truncating any site with a value of p less than 0.0158 down to a value of zero.

The corresponding spacing distribution between occupied sites as determined by the DPSP model and experimental data is shown in figure 7. The experimental data was taken from NMR data on a 3D lattice. The expressions for $\hat{q}$ in equation (2) is modified by a factor of $\frac{1}{150}$ to ensure that integration of the probability field over the entire domain at the desired density is normalized. Despite the difference in the dimensionality, *i.e.* a 2D computation compared with measurements of a 3D system, it is a validation of this approach that the qualitative and quantitative values for the distribution are similar in the experimental and 2D DPSP simulation.

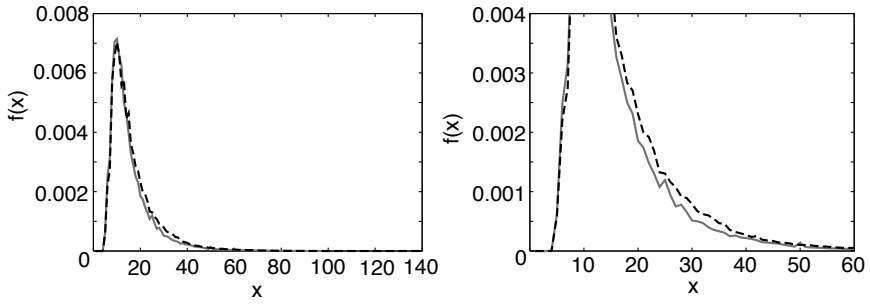

Figure 7: Spacing distribution corresponding to the 10,000 x 10,000 site lattice. The left image is the distribution over the range of spacing values; the right image is a close up of the same distribution. The experimental data is for a 3D lattice and is represented by the solid line and the dashed line represents the DPSP model result.

An alternate expression for $\hat{q}$ has also been examined:

$$\hat{q}\,(r_i) \equiv \begin{cases} 0 & \text{if } r_i < 1, \\ 1 - \exp\left[-\frac{(r_i-1)^2}{2}\right] & \text{if } 1 \le r_i \le S, \\ 1 & \text{if } r_i > S. \end{cases} \tag{3}$$

This exponential function results in larger values of p for neighboring sites to an occupied site. While the physical significance of this expression in unclear, it may become useful if specific mechanisms can be connected to the nucleation process. Future simulations will be performed to compare the traits of this function with the earlier one given.

Although the growth model has not been implemented, the basic framework has been established. At the conclusion of the nucleation stage, a file is stored recording the nucleation sites. At present, it is assumed that the bubbles grow in a uniform radial pattern. For example, if the bubbles grow at the rate of r units per time step, after n growth steps, the bubble contains all sites within radius n of a nucleation site. After each step an analysis of the lattice is conducted in which the spacing distribution, cluster sizes and whether channel formation has occurred is recorded. Since the bubble growth rate is uniform across the lattice, the number of growth steps required for bubbles emanating from the root sites can be found using the index values for each nucleation site. Using the same example as above, denote 3 sites, $\{p_i\}$, $i = 1, 2, 3$ and d_{ij} to be the distances between p_i and p_j. Then, the bubbles formed by p_i and p_j merge after $\lceil r(d_{ij}-1)/2 \rceil$ steps where $\lceil x \rceil$ represent the smallest integer $\geq x$. The order in which bubbles merge is recorded during the simulation, as is the time at which channel formation across the lattice is achieved. As stated earlier, the fidelity of this growth process can be improved by including scaling of the growth rate according to the spacing between a given root and its neighbors, which we associate with source volume for the root bubble.

This page intentionally left blank.

5 Fractal Model of Percolation

A modern treatment of percolation theory has emerged from the study of fractals. A detailed description of the fractal model can be found in [29] and [30]. For the purposes of this paper, attention is focused on the two dimensional case. Earlier, we defined a percolation cluster as a cluster that forms a channel that connects the boundaries of the medium. The symbol $M(L)$ denotes the number of sites that belong to the largest cluster on the LxL sublattice. It is desirable to know how $M(L)$ varies as a function of L. For $p > p_c$ $M(L)$ increases almost linearly with the area of the frame, L^2. Hence, $M(L) \sim P_N(p)L^2$. For the limit of $L \to \infty$, this tends to $P_\infty(p)L^2$ where $P_\infty(p)$ is simply the density of sites belonging to the percolating cluster. For $p < p_c$ we expect $M(L)/L^2 \to 0$ as $L \to \infty$. At $p = p_c$, one expects $M(L)$ to increase almost as L^2. Thus, from numerical experiments,

$$M(L) \sim_{L\to\infty} \begin{cases} \log L, & p < p_c \\ L^D, & p = p_c \\ L^E, & p > p_c. \end{cases}$$

Thus, at $p = p_c$ $M(L)$ grows as a power law, L^D, where D is the fractal dimension, while $M(L)$ grows as L^E, where E is the Euclidean dimension of the lattice, for $p > p_c$. This shows that the percolation cluster is fractal with fractal dimension D at the threshold. Current numerical evidence suggests that $D = 91/48 \sim 1.89583$ for all 2-dimensional lattice site percolation problems. Thus, we may conclude that the mass of the cluster increases on the average with L as

$$M(L) \sim \overline{A} L^D, \tag{4}$$

where $D = 91/48$ and $\overline{A}$ is the effective amplitude estimated over finite size samples. Note that this estimate is valid only for asymptotically large L. For "realistic" L values, the estimate can be modified using correction terms derived by transfer matrix methods [31]. It is interesting to note that the Mandelbrot-Given curve has fractal dimension $D = 1.892....$

A characteristic of the fractal model is self-similarity. That is, if one picks a random location on the profile of the fractal, then the macroscopic geometry is replicated at smaller scales as one approaches the point. As seen in [29], the percolation cluster is statistically self-similar. This assertion can be made quantitative by a technique called real space renormalization. This concept is best shown by considering a 2-dimensional triangular lattice as shown in figure 8. Previous results have shown that $p_c = 0.5$ and $D = 91/48$. Regroup the sites as follows: basic cells of $b^2 = 3$ sites are replaced by single new sites which are considered to be occupied if a majority of the sites in the cell are occupied. This changes the scale of the lattice by a factor of $b = \sqrt{3}$. The new lattice has new concentration p' of occupied sites where

$$p' = \underbrace{p^3}_{\text{probability of finding 3 occupied sites}} + \underbrace{3p^2(1-p)}_{\text{probability of finding 2 occupied sites}}. \tag{5}$$

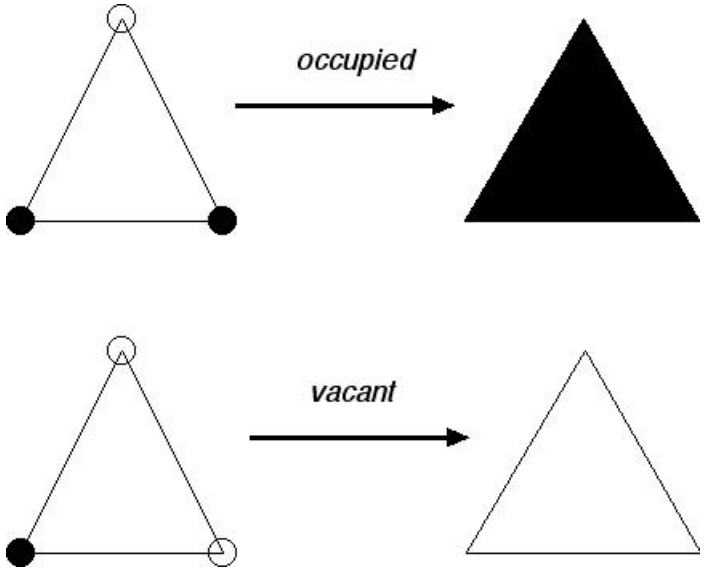

Figure 8: Example of real space renormalization with respect to a single triangle lattice element. If the majority of nodes is occupied, the entire cell is considered to be an occupied node in the renormalized lattice. If the majority are empty, the cell is taken to be vacant.

Note that $p = p_c$ solves the iteration equation 5. In fact, p_c is a fixed point of the renormalization transformation (of course, $p = 0, 1$ are also fixed points.) At the percolation threshold, the scaling law (4) applies for the cluster obtained after scaling by a factor b. But the linear size of the scaled lattice is only L/b. Therefore, $M(L/b) \sim \overline{A}(L/b)^D$. Hence, $M(L) = b^D M(L/b)$. This implies that $M(L)$ must have power law structure. Thus, the percolation cluster has self similarity and fractal geometry. Note that this argument is valid asymptotically for large L and L/b but valid for all b.

At percolation, there exists a wide distribution of cluster sizes. As p is decreased below p_c, the cluster sizes decrease. Above p_c, there are clusters of various sizes in the holes of the percolating cluster. Denote s to be the number of sites in a cluster [1] and let $R_g(s)$ be the radius of gyration of a cluster having s sites. This is defined as the root mean square radius of the cluster measured from its center of gravity. When a finite cluster (at p_c) is analyzed inside a box with side $L \leq 2R_g(s)$, then it appears to be a part of the incipient percolation cluster spanning the box. One finds $M_s(L) \sim L^D$ (as usual.) However, when the box size is increased beyond $2R_g$, the cluster edges come into view. For sufficiently large L the entire cluster fits inside L_s. As L increases, $M(L)$ does not increase. The mass, $M_s(L)$, inside the box of size L on a cluster consisting of s sites is given by

$$M_s(L) = L^D f\left(\frac{L}{R_g}\right) \rightarrow \begin{cases} \overline{A}(L/R_g)^D, & L << R_g(s) \\ s, & L >> R_g(s). \end{cases} \tag{6}$$

[1] Note that this is different from $M(L)$. Recall that $M(L)$ is the number of sites in the *largest* cluster.

Notice that $f(x) \to \overline{A}$ as $x = L/R_g(s) \to 0$. However, $M_s(L)$ must be independent of L for $x >> 1$. So, $f(x) \sim x^{-D}$ (Why? So L^D is cancelled in (6)). Hence,

$$s = M_s\,(L >> R_g) \sim L^D\,(L/R_g)^{-D} \sim R_g^D. \tag{7}$$

The preceding analysis is independent of whether the classical or dynamic percolation method is used. As such, it is expected that the DPSP model will also yield a fractal percolation cluster. How the dynamic qualities will affect the fractal dimension is one of the many aspects still to be investigated.

It is interesting to note that elements of this fractal approach related to dimensional invariants have already been applied to the bubble nucleation problem. Classical percolation theory predicts that infinite percolation occurs at a critical volume fraction of 0.15 for a three dimensional lattice [11]. This value can be used with the relation in (7) and a fractal dimension of $D = 2.5$ to evaluate how cluster radius and particle (system) size effect the helium-to-metal ratio at the point of accelerated release of He gas.

This page intentionally left blank.

6 Conclusion

A dynamic point-source percolation (DPSP) model was presented. This model is based on classical percolation theory, but allows for an evolving probability field for the selection of unoccupied sites to be filled and has the capability to include distinct mechanisms for site selection that are representative of physical processes. Generalized crystal geometries were considered by mapping to a geometrically simple lattice. Doing so allowed all geometrical data to be found analytically, resulting in a process to recall geometric data that is more efficient than calculation or accessing memory.

Using the physical model of He bubble growth as a basis, the DPSP model created two distinct site occupation algorithms to correspond to the bubble nucleation and growth stages. Testing of the model was accomplished by simulating the nucleation phase of bubbles within a two dimensional lattice. Comparison of the spacing distribution at the conclusion of the nucleation stage with experimental results obtained with NMR is good and validates the DPSP approach, despite the mismatch in dimensionality of the computational and physical domains. A methodology for simulating the growth of nucleated He bubbles was developed and presented, although implementation of this method has yet to be accomplished.

This report presented not only a thorough background on both classical percolation theory and a detailed explanation of how the DPSP model deviates from the classical theory, but also provided information on a more modern treatment of percolation using the study of fractals. Use of this technique within the framework of the existing DPSP model is delegated for future development, but is worthwhile in assessing the impact of the various length scales present in material systems, *e.g.* lattice spacing, grain size, powder particle size, etc., on the ability of the DPSP model to predict the accelerated release of He gas.

Another avenue for future development of the DPSP model is the direct replacement of stochastic features with physically-based processes. For example, the inclusion of anisotropic characteristics of the percolating medium, and it's effect on bubble growth needs to be included. Also, implementation of conditions leading to the termination of bubble nucleation within the DPSP algorithm is required. As indicated above, while the two dimensional model provided acceptable results, a full 3D simulation will be necessary for accurate representation of physical systems. Finally, the nucleation stage of the DPSP model is performed in a random fashion, in accordance with the mechanism of self-trapping of He atoms. It would also be desirable to model the nucleation and growth of bubbles formed along defects, such as dislocations, that already exist within the system prior to tritium decay or He implantation. These defects may not be distributed randomly and methods for altering the nucleation probability field to account for their presence need to be developed and implemented.

This page intentionally left blank.

7 References

[1] R. Causey. Interaction of helium with dislocations in metals: Mini review. 2001.

[2] S. Thiébaut, B. Décamps, J.M. Pénisson, B. Limacher, and A. Percheron Guégan. TEM study of the aging of palladium-based alloys during tritium storage. Journal of Nuclear Materials, 277:217–225, 2000.

[3] A. Ryazanov, H. Matsui, and A.V. Kazaryan. Physical mechanisms of helium release during deformation of vanadium alloys doped with helium atoms. Journal of Nuclear Materials, 271&272:356–359, 1999.

[4] G.C. Abell, L.K. Matson, R.H. Steinmeyer, R.C. Bowman Jr., and B.M. Oliver. Helium release from aged palladium tritide. Physical Review B, 41(2):1220–1223, 1990.

[5] J.A. Emig, R.G. Garza, L.D. Christensen, P.R. Coronado, and P.C. Souers. Helium release from 19-year-old palladium tritide. Journal of Nuclear Materials, 187:209–214, 1992.

[6] D. Stauffer and A. Aharony. Introduction to Percolation Theory. Taylor & Francis, 1992.

[7] S.R. Broadbent and J.M. Hammersley. Percolation processes, i. crystals and mazes. Proceedings of Cambridge Philosophical Society, 53:629–641, 1957.

[8] S. Kirkpatrick. Percolation and conduction. Reviews of Modern Physics, 45(4):574–588, 1973.

[9] H.T. Weaver and W.J. Camp. Detrapping of interstitial helium in metal tritides—NMR studies*. Physical Review B, 12(8):3054–3059, 1975.

[10] W.J. Camp. Helium detrapping and release from metal tritides. Journal of Vacuum Science and Technology, 14(1):514–517, 1977.

[11] R.G. Jr. Spulak. On helium release from metal tritides. Journal of the Less-Common Metals, 132:L17–L20, 1987.

[12] C. Ronchi. Physical processes and meschanisms related to fission gas swelling in MX-type nuclear fuels. Journal of Nuclear Materials, 84:55–84, 1979.

[13] A. R. Massih. Percolation model for bubble interlinkage in ceramic nuclear fuels. Journal of Nuclear Materials, 119:116–118, 1983.

[14] V.K.S. Shante and S. Kirkpatrick. An introduction to percolation theory. Advanced Physics, 20(85):325–357, 1971.

[15] R.M. Ziff. Test of scaling exponents for percolation-cluster perimeters. Physical Review Letters, 56(6):545–548, 1986.

[16] S. C. van der Marck. Site percolation and random walks on d-dimensional kagome lattices. Journal of Physics A, 31:3449–3460, 1998.

[17] M.F. Sykes and J.W. Essam. Exact critical percolation probabilities for site and bond problems in two dimensions. Journal of Mathematical Physics, 5(8):1117, 1964.

[18] C. d'Iribarne, M. Rasigni, and G. Rasigni. Minimal spanning tree and percolation on mosaics: graph theory and percolation. Journal of Physics A, 32:2611–2622, 1999.

[19] A. Rosowsky. An analytical method to compute an approximate value of the site percolation threshold p_c. European Physical Journal, B(15):77–86, 2000.

[20] M.P. Allen and D.J. Tildesley. Computer Simulation of Liquids. Clarendon Press, Oxford, 1987.

[21] S. A. Bagnich and A.V. Konash. The influence of inhomogeneous properties of a system on the percolation process in two-dimensional space. Physics of the Solid State, 43(12):2313–2320, 2001.

[22] J.E.P. Monteagudo, R. Krishnaswamy, and P.L.C. Lage. Scaling laws in network models: porous medium property prediction during morphological evolution. Journal of Petroleum Science and Engineering, 32:179–190, 2001.

[23] J. Hoshen and Kopelman R. Percolation and cluster distribution. i. cluster multiple labeling technique and critical concentration algorithm. Physical Review B, 14(8):3438–3445, 1976.

[24] M.E.J. Newman and R.M. Ziff. Efficient monte carlo algorithm and high-precision results for percolation. Physical Review Letters, 85(19):4104–4107, 2000.

[25] M.E.J. Newman and R.M. Ziff. Fast monte carlo algorithm for site or bond percolation. Physical Review E, 66(1):016706/1–10, 2001.

[26] R. Sedgewick. Algorithms in C++. Addison-Wesley, 1992.

[27] W.D. Wilson, C.L. Bisson, and M.I. Baskes. Self-trapping of helium in metals. Physical Review B, 24(10):5616–5624, 1981.

[28] D.F. Cowgill. private communication, 2003.

[29] J. Feder. Fractals. Plenum Press, 1988.

[30] T. Vicsek. Fractal Growth Phenomena. World Scientific, 1992.

[31] X.R. Wang. The transfer matrix approach to the self-avoiding walk in fractal spaces. Physica A, 205:391–398, 1994.

8 DISTRIBUTION:

1	MS 0316	J.B. Aidun, 9235
1	MS 0335	R.G. Spulak, 2564
1		M.A. Mangan, 14405
1		C.S. Snow, 2564
1	MS 0521	F.M. Bacon, 2502
1	MS 0841	T.C. Bickel, 9100
1	MS 0847	H.S. Morgan, 9120
1	MS 0867	J.F. Browning, 14405
1	MS 0871	L.C. Beavis, 14402
1	MS 0885	G.S. Heffelfinger, 1802
1	MS 0886	P.G. Kotula, 1822
1	MS 1056	B.L. Doyle, 1111
1	MS 1411	H.E. Fang, 1834
1		S.M. Foiles, 1834
1		J.J. Hoyt, 1834
1	MS 1427	J.M. Phillips, 1100
1	MS 9001	M.E. John, 8000 Attn: R.H. Stulen, 8100, MS 9004 D.R. Henson, 8200, MS 9007 W.J. McLean, 8300, MS 9054 K.E. Washington, 8900, MS 9003
1	MS 9052	S.F. Rice, 8367
1	MS 9108	R.D. Monson, 8243
1		C.A. Lajeunesse, 8243
1		C.W. Pretzel, 8243
1		S.L. Robinson, 8243
1		G.C. Story, 8243
1	MS 9161	E.P. Chen, 8763

1		P.A. Klein, 8763
30		J.A. Zimmerman, 8763
1	MS 9202	R.M. Zurn, 8205
1	MS 9402	C.H. Cadden, 8772
1		R. Causey, 8772
10		D.F. Cowgill, 8772
1		K.L. Hertz, 8772
1		B.P. Somerday, 8772
1	MS 9403	J.C.F. Wang, 8773
1		A.J. Antolak, 8773
1		E.H. Majzoub, 8773
1		D.H. Morse, 8773
1	MS 9405	J.M. Hruby, 8700 Attn: G.D. Kubiak, 8750, MS 9404 C.D. Moen, 8752, MS 9042 J.R. Garcia, 8754, MS 9409 W.R. Even Jr., 8760, MS 9161 D.L. Medlin, 8761, MS 9161 T.J. Shepodd, 8762, MS 9403 P.A. Spence, 8774, MS 9042
1	MS 9405	K.L. Wilson, 8770
1	LANL	B.A. Meyer,ESA-GTS, C934
1		K.G. Honnell, ESA-GTS, C934
1	LLNL	W.G. Wolfer,L353
1		C.R. Krenn, L353
1		A.J. Schwartz, L353
1		K.A. Winer, L170
1	MS 0899	Technical Library, 9616
3	MS 9018	Central Technical Files, 8945-1
1	MS 9021	Classification Office, 8511/ Technical Library, MS 0899, 9616
1		DOE/OSTI via URL